
Article:
Angelova, D. and Mihaylova, L. (2011) Contour segmentation in 2D ultrasound medical images with particle filtering. Machine Vision and Applications, 22 (3). 551 - 561. ISSN 0932-8092

https://doi.org/10.1007/s00138-010-0261-4

Machine Vision and Applications manuscript No.
(will be inserted by the editor)

Contour Segmentation in 2D Ultrasound Medical Images with Particle Filtering

Donka Angelova · Lyudmila Mihaylova

Received: date / Accepted: date

Abstract - Object segmentation in medical images is an actively investigated research area. Segmentation techniques are a valuable tool in medical diagnostics for cancer tumors and cysts, for planning surgery operations and other medical treatment. In this paper a Monte Carlo algorithm for extracting lesion contours in ultrasound medical images is proposed. An efficient multiple model particle filter for progressive contour growing (tracking) from a starting point is developed, accounting for convex, non-circular forms of delineated contour areas. The driving idea of the proposed particle filter consists in the incorporation of different image intensity inside and outside the contour into the filter likelihood function. The filter employs image intensity gradients as measurements and requires information about four manually selected points: a seed point, a starting point, arbitrarily selected on the contour, and two additional points, bounding the measurement formation area around the contour. The filter performance is studied by segmenting contours from a number of real and simulated ultrasound medical images. Accurate contour segmentation is achieved with the proposed approach in ultrasound images with a high level of speckle noise.

Research supported in part by the Bulgarian Foundation for Scientific Investigations, Grant TK 01-200/2009

Donka Angelova
Institute for Parallel Processing,
Bulgarian Academy of Sciences
Tel.: + 359 2 9796622
Fax: + 359 2 870 72 73
E-mail: donka@bas.bg

Lyudmila Mihaylova
Department of Communication Systems, Lancaster University,
Tel.: 01524 510388
Fax: +123-45-678910
E-mail: mila.mihaylova@lancaster.ac.uk

Keywords Ultrasound (US) image segmentation · Contour tracking · Bayesian inference · Sequential Monte Carlo methods · Particle filter (PF), speckle noise

1 Introduction

Automated or semi-automated contour extraction is one of the most challenging image processing tasks, pertaining to a great variety of applications. In particular, a segmentation method that could accurately delineate the lesion contours in medical images is of significant importance for diagnostics, image-guided interventions and therapy. Due to the relatively low quality of clinical images, the task of contour segmentation is rather complex. This motivates the considerable interest in segmentation of medical images (please see [28, 41] and references therein).

There is a great deal of approaches for medical image segmentation such as active contour models [8, 16, 25,26], expectation-maximisation [38], principal component analysis [9, 32], networks and learning combined, texture and morphologic information in various interpretations [12,17,22], level sets [10], and Bayesian techniques [14, 15, 23, 24]. In general, the methods can be classified in two groups of optimisation techniques: 1) off-line techniques - quite accurate, but computationally demanding, and 2) on-line fast algorithms, less precise, but implementable nearly in real time.

Every method has its relevant place in the variety of technologies developed for medical imaging: radiography [38], computer tomography (CT) [12,40], magnetic resonance (MR) [9, 14, 16, 22, 23, 36], breast thermography, photoacoustic imaging and ultrasonography. Ultrasonography has a special place amongst medical imag-

ing techniques. While it may provide less anatomical detail than techniques such as CT or MR, it has several advantages which make it suitable for numerous applications: imaging the fetus, abdominal organs, heart, breast, muscles, tendons, arteries and veins. It is very safe to use and does not appear to cause any adverse effects. Ultrasound imaging is relatively inexpensive and quick to perform. Doppler capabilities allow the blood flow in arteries and veins to be assessed.

The aim of this work is to develop an approach for fast US image segmentation, possessing high estimation accuracy achievable at reasonable computational cost. A powerful approach, avoiding many drawbacks of the optimisation procedures, consists in consecutively growing (tracking) of a contour from a starting point according to a certain criterion of efficiency. Our choice of the Bayesian methodology is motivated by its power to solve problems with uncertainties, high level of noises and ability to account for the prior information, as shown in numerous applications surveyed in [28] and [37]. At the same time as pointed out in [28] *the high-quality segmentation method needs to make use of all task-specific constraints or priors.*

A number of successful contour determination algorithms are published in the specialised literature, implementing tracking techniques with a different level of complexity. For example, a Kalman filter with an adaptive measurement association gate is proposed in [34], being a part of a multi-stage procedure for prostate border estimation. The Kalman filter is also applied to detecting bone edges in [40]. The concept of multiple hypothesis tracking (MHT) is particularly useful for simultaneous tracking of multiple potential contours, avoiding the loss of the true one at the places of uncertainty.

Tracking methods are adopted also in [1] for the purposes of heart chambers and breast cyst segmentation. The recursive contour growing (motion) is governed by a finite set of switching dynamical models and thus its behavior can be probabilistically predicted. Candidate edge points, obtained around the predicted contour, represent both a measurement of the true contour position and some false returns. The concept of combining multiple trajectory models in order to estimate the state of manoeuvring object in clutter has its rational solution in the face of combining the interacting multiple model (IMM) estimator and a probabilistic data association filter (PDAF) [6]. The authors of [1, 2] demonstrate the accuracy of their IMM-PDAF implementation by segmenting convex, non-circular lesion forms over a number of prostate, carotid artery, jugular vein ultrasound images. The IMM-PDAF results show that the multiple hypothesis approach jointly applied with multiple switching motion models yields correct and convergent contour tracking in the complicated medical imaging environment.

In contrast with the MHT and IMM-PDA estimators, which belong to the class of *analytical approximations* to the optimal Bayesian solution, the *sampling (Monte Carlo) approximations* offer more accurate representation of multi-modal distributions, inherent to medical images. Particle filters (PFs) afford maintaining multiple hypotheses in a very compatible and simple manner. Also, constraints on curvature and features of the application can be incorporated into the tracking framework in an easy and natural way.

A robust particle filtering algorithm for contour following is developed in [30]. The potential of this algorithm (called JetStream) is demonstrated in the context of the interactive cut-out in photoediting applications.

JetStream is a general tool for designing contour tracking algorithms in different application areas. The designer has the freedom to choose appropriate task oriented ingredients: dynamics and measurement models, likelihoods or likelihood ratios and constraints. Based on the JetStream ideas, an algorithm for rotoscoping is proposed in [31]. The authors suggest an oriented particle spray to deal with sharp contour angles. They design a directional probability density function that is better able to control the evolution of the contour.

This paper develops a new segmentation algorithm for ultrasonic images and at the same time extends some of the capabilities of JetStream for efficient and reliable US segmentation. The new elements of the proposed algorithm, compared with JetStream, include: 1) a multiple model structure that captures the prior dynamics, and governs the growing process of the predicted contour; 2) a combined likelihood is proposed involving the intensity gradients along x, y axes and the radii, projected from the seed point towards the contour; 3) incorporation of constraints accounting for the contour convexity.

A high quality segmentation algorithm should provide fully automated contour extraction, without an operator's intervention. There exist a number of techniques for image partitioning, localising the areas and points of interests [11,28,34]. Some of them combine conventional intensity-based thresholding with fuzzy logic and elaborated decision making rules under uncertainty. However, the quality of automatic segmentation highly depends on the homogeneity of the background and foreground intensity distributions. Also, the feasibility of the algorithms is often limited to a certain class of clinical applications. In contrast with these algorithms we propose a semi-automated approach, motivated by the

necessity of real-time applications to a broad range of contour segmentation problems. The positions of four manually selected points are required: a seed point, a starting point and two additional points, bounding the measurement formation area around the contour. In some medical applications, where additional information is available, the proposed approach can make use of two points only and hence to reduce in this way the operator intervention, similarly to [1, 2].

In order to reduce the effect of speckle noises and to improve the image contrast, median filtering, smoothing and other pre-filtering techniques are an inherent part of many segmentation approaches for ultrasound medical images [28]. For example, the authors of [10] suggest stepped anisotropic diffusion filtering, stick method and automatic thresholding, based on the threshold-determination algorithm of Otsu [29]. In our approach, a non-linear Gaussian filter, performing edge preserving diffusion is applied [3, 5].

The paper is organised as follows. Section 2 formulates the problem of contour following as a task of tracking and outlines its approximate solution by particle filtering. The proposed multiple model particle filter is presented in Section 3. The stages of the algorithm: preprocessing, filtering and smoothing, are briefly outlined in Section 4. Section 5 validates the performance of the algorithm over real and simulated medical ultrasound images characterised with high level of speckle noise. Comments and conclusions are finally given in Section 6.

2 Contour Following as a Task of Tracking

Denote by $\boldsymbol{y}$ the observed image, which is a source of all measurements, available to the contour estimator. Consider a state vector $\boldsymbol{x}$, containing points $\boldsymbol{x}_k$ in the image plane. Any ordered sequence $\boldsymbol{x}_{0:n} \equiv (\boldsymbol{x}_0, \ldots, \boldsymbol{x}_k, \ldots, \boldsymbol{x}_n)$ defines uniquely the contour being tracked [30]. Given a prior dynamics $p(\boldsymbol{x}_{k+1}|\boldsymbol{x}_{0:k})$, modeling the expected evolution of the contour, *the aim is to enlarge the sequence* $\boldsymbol{x}_{0:k}$, using the measurement data $\boldsymbol{y}$.

This can be achieved by recursively calculating the posterior state probability density function (pdf)

$$p_{k+1}(\boldsymbol{x}_{0:k+1}|\boldsymbol{y}) \propto p(\boldsymbol{y}|\boldsymbol{x}_{k+1}) p(\boldsymbol{x}_{k+1}|\boldsymbol{x}_k) p_k(\boldsymbol{x}_{0:k}|\boldsymbol{y}), \quad k = 0, 1, \ldots, n-1, \tag{1}$$

where $p(\boldsymbol{y}|\boldsymbol{x}_{k+1})$ corresponds to the data model. Often $\boldsymbol{y}(\boldsymbol{x}_k)$ is the gradient norm $|\nabla I(\boldsymbol{x}_k)|$ of image intensity. The starting point $\boldsymbol{x}_0$ can be chosen manually or automatically.

Then the contour extraction problem, expressed as a minimisation of the function

$$\Im_n(\boldsymbol{x}_{0:n}, \boldsymbol{y}) \equiv -log\, p_n(\boldsymbol{x}_{0:n}|\boldsymbol{y}), \tag{2}$$

can be solved by finding the maximum a posteriori (MAP) estimate (or the expectation) of the posterior state pdf [7, 35].

The recursion (1) cannot be computed analytically. Within the sequential Monte Carlo framework, the posterior density function $p_k(\boldsymbol{x}_{0:k}|\boldsymbol{y})$ is approximated by a finite set $\left\{\boldsymbol{x}_{0:k}^{(j)}\right\}$, $j = 1, \ldots, N$ of N sample paths (particles). The generation of samples from $p_{k+1}(\boldsymbol{x}_{0:k+1}|\boldsymbol{y})$ is performed in two steps of prediction and update, thoroughly described in the specialised literature [13]. At the prediction step, each path $\boldsymbol{x}_{0:k}^{(j)}$ is grown of one step $\widetilde{\boldsymbol{x}}_{0:k+1}^{(j)}$ by sampling from the proposal density function $p(\boldsymbol{x}_{k+1}|\boldsymbol{x}_k^{(j)})$. At the step of update, each sample path is associated with a weight, proportional to the likelihood of the measurements

$$w_{k+1}^{(j)} \propto w_k^{(j)} p(\boldsymbol{y}(\widetilde{\boldsymbol{x}}_{k+1}^{(j)})). \tag{3}$$

The resulting set of weighted paths (contours) $\left\{\widetilde{\boldsymbol{x}}_{0:k+1}^{(j)}, \tilde{w}_{k+1}^{(j)}\right\}$, $j = 1, \ldots, N$ with normalised weights $\tilde{w}_{k+1}^{(j)} = w_{k+1}^{(j)} / \sum_{j=1}^{N} w_{k+1}^{(j)}$, provides an approximation to the distribution $p_{k+1}(\boldsymbol{x}_{0:k+1}|\boldsymbol{y})$.

When an estimate of the effective sample size $N_{eff} = 1/\sum_{j=1}^{N} \left(\tilde{w}_k^{(j)}\right)^2$ falls below a threshold N_{thresh}, resampling is realised to avoid possible degeneracy of the sequential importance sampling [13]. In the resampling step N paths $\left\{\boldsymbol{x}_{0:k+1}^{(j)}, w_{k+1}^{(j)}\right\}$, $j = 1, \ldots, N$ are drawn with replacement from the previous weighted set, where $w_{k+1}^{(j)} = 1/N$.

Based on the discrete approximation of the posterior state pdf $p_{k+1}(\boldsymbol{x}_{0:k+1}|\boldsymbol{y})$, an estimate of the "best" path (contour) at step $k+1$ can be obtained. The mean

$$\mathbb{E}(\boldsymbol{x}_{0:k+1}|\boldsymbol{y}) \approx \sum_{j=1}^{N} \widetilde{w}_{k+1}^{(j)} \widetilde{\boldsymbol{x}}_{0:k+1}^{(j)} \tag{4}$$

represents a Monte Carlo approximation of the posterior pdf expectation. This technique provides sample-based approximations of posterior distributions with almost no restriction on the ingredients of the models.

3 A Multiple Model Particle Filter for Contour Extraction

The models of prior dynamics and measurement data should provide growing of a contour, avoiding slowing down and interruption of the process [30]. This is closely

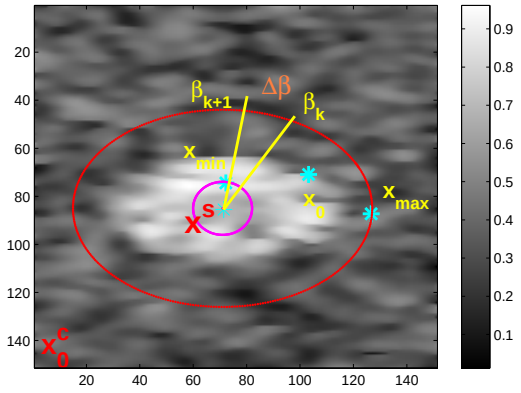

Fig. 1 An ultrasound image with a center of the contour $\boldsymbol{x}^s$. The object to be segmented is bounded by an ellipse.

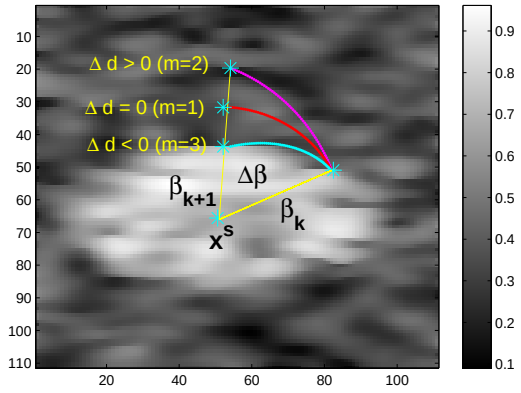

Fig. 2 The distance increments for different modes.

related with the selection of a variable that is analogous to the time variable, since the notion of time is associated with the successive contour growing. It is natural to assume a fixed time analog: for an arc-length or for an angle and the choice of a step is application dependent. The measurement data are usually characterised by grey level distributions and/ or intensity gradients (and higher derivatives). The formation of the measurement space is constrained by the probabilistic gating procedure, applied in tracking techniques [1, 6]. In the present paper, the gate space is imposed on the image plane by hard constraints. The details of filter design are given below.

3.1 Prior Dynamics

We consider the typical case of lesions with a convex form, where all contour points can be seen from a seed point inside the lesion cavity [1]. If n equispaced radii are projected from the seed point towards the contour, then an appropriate variable, analogous to the time step is the angle between the adjacent radii $\triangle\beta = 2\pi/n$. Since the delineated area can have an arbitrary (non-circular) shape, a multiple model (hybrid) dynamics is adopted, describing the contour evolution from angle β_k to angle $\beta_{k+1} = \beta_k + \triangle\beta$, $k = 0, \ldots, n$. Let $\boldsymbol{x}^s = (x^s,\, y^s)'$ be the location of the seed point in the Cartesian coordinate frame, centered at the left and low corner $\boldsymbol{x}_0^c = (x_0^c,\, y_0^c)'$ of the image (as shown on Fig. 1). Let $\boldsymbol{d} = (d,\, \beta)'$ be the location of an arbitrary image point in the relative polar coordinate system, centered at the seed point.

The following *discrete-angle jump Markov model*

$$\boldsymbol{d}_{k+1} = \boldsymbol{F}\boldsymbol{d}_k + \boldsymbol{G}\boldsymbol{u}_{k+1}(m_{k+1}) + \boldsymbol{B}\mathrm{w}_{k+1}(m_{k+1}), \qquad (5)$$

can describe the contour where $\boldsymbol{d}_k = (d_k,\, \beta_k)'$ is the base (continuous) state vector, representing contour point coordinates along the radius, determined by β_k, $\boldsymbol{F}$ is the state transition matrix and $\boldsymbol{u}_k$ is a known control input. The process noise $\mathrm{w}_k(m_k)$ is a white Gaussian sequence with known variance: $\mathrm{w}_k \sim \mathcal{N}(0, \sigma_d^2(m_k))$. The modal (discrete) state $m_k \in \mathbb{S} \triangleq \{1,\ 2, \ldots,\ s\}$, characterising different contour behaviour modes, is evolving according to a Markov chain with known initial and transition probabilities

$$\pi_{ij} \triangleq Pr\left\{m_{k+1} = j \mid m_k = i\right\},\ (i, j \in \mathbb{S}).$$

The control input $\boldsymbol{u}_k(m_k) = (\triangle d_k(m_k),\, \triangle\beta)'$ is composed of the distance increment $\triangle d_k(m_k)$ and sampling angle $\triangle\beta$. In the present implementation the set of modes $\mathbb{S}$ contains three models ($s = 3$). The first mode ($m = 1$) corresponds to zero increment ($\triangle d_k = 0$). It models the "move" regime along the circle. The non-zero increments ($\triangle d_k > 0$ for $m = 2$) and ($\triangle d_k < 0$ for $m = 3$) are constants corresponding to distance increase or decrease, respectively (Fig. 2). The process noise w_k models perturbations in the distance increment. The matrices $\boldsymbol{F}, \boldsymbol{G}$ and $\boldsymbol{B}$ have a simple form

$$\boldsymbol{F} = \boldsymbol{G} = \begin{pmatrix} 1 & 0 \\ 0 & 1 \end{pmatrix}, \quad \text{and} \quad \boldsymbol{B} = \begin{pmatrix} 1 & 0 \end{pmatrix}'.$$

In this model, the state vector $\boldsymbol{x}_k = (x_k, y_k, d_k, \beta_k)'$ contains both the Cartesian coordinates of a contour point with respect to the left-down image corner and the polar coordinates with respect to the internal seed point.

3.2 Constraints

Taking into account the proposed convex form of the contour, the area of measurement formation is bounded

by an inner circle and an outer ellipse (as shown on Fig. 1). Two points, $\boldsymbol{x}_{min}$ and $\boldsymbol{x}_{max}$, selected manually, determine the gating area. The distances d_{min} and d_{max} of the points in the polar coordinate system correspond respectively to the circle radius R_c and the major semi-axis of the ellipse Re_{max}. The variable $\gamma = Re_{max} - R_c$ is used as a design parameter. It can be viewed as a kind of aspect ratio. The minor semi-axis of the ellipse is calculated according to the relationship: $Re_{min} = R_c + 2/3Re_{max}$.

Suppose that a cloud of N particles $\left\{\widetilde{\boldsymbol{x}}_{k+1}^{(j)}\right\}, j = 1, \ldots, N$ is predicted at the angle β_{k+1} according to the state evolution equation (5). At this stage, constraints are imposed on particles falling outside the boundaries, and these particles are forced to accept the coordinates of the boundaries. Then, the likelihood is computed for each particle point, situated inside and on the boundaries.

3.3 Likelihood

The likelihood $p(\boldsymbol{y}|\boldsymbol{x}_k)$ in the relationship (1) has different forms, depending on the authors' considerations and application particularities. In most cases, the gradient norm $|\nabla I(\boldsymbol{x}_k)|$ of image intensity I is a principal likelihood component. We explore three likelihood alternatives.

Likelihood I. Denote by $p_{on} \equiv p_{on}(\boldsymbol{y}(\boldsymbol{x}_k)|\boldsymbol{x}_{0:n})$ the likelihood of the pixel $\boldsymbol{x}_k$, if it belongs to the contour $\boldsymbol{x}_{0:n}$. Denote also by $p_{off} \equiv p_{off}(\boldsymbol{y}(\boldsymbol{x}_k))$ the likelihood of the same pixel, if it does not belong to the contour. According to [30] the likelihood ratio

$$\ell = p_{on}/p_{off}, \quad \ell \propto p(\boldsymbol{y}(\boldsymbol{x}_k))$$

is a measure, extracting useful information from the image data. Following the methodology, suggested in [30], we have explored the gradient norm distribution both off contours (p_{off}) and on contours (p_{on}) over a series of images. The empirical distribution of the gradient norm off contours (on the whole image data) confirmed the results, obtained in [30]. The gradient norm distribution can be approximated by an exponential distribution with parameter λ, which is the average gradient norm (as shown on Fig. 3 (a)). However, the empirical distribution p_{on} of the joint gradient norm and gradient direction on the contour, obtained and implemented in [30], do not provide enough information for accurate contour extraction in ultrasound images.

We adopt an approach of combining the gradient norm and an edge detection algorithm, proposed in [1]. The aim is to incorporate *simultaneously* the gradient

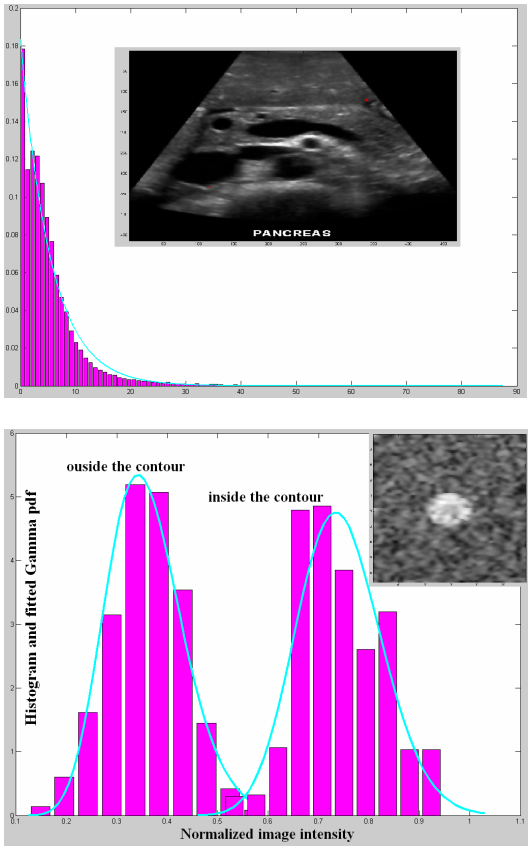

Fig. 3 (a) Normalised histogram of gradient norm on the whole image and the fitted exponential pdf; (b) Normalised intensity histograms for the parts inside and outside the contour, respectively, and the fitted Gamma pdfs

information along x, y axes, and along the radii, projected from the seed point toward the contour, in order to improve the edge detection sensitivity.

Note that N predicted particles $\left\{\widetilde{\boldsymbol{x}}_{k+1}^{(j)}\right\}, j = 1, \ldots, N$ are located along the radius, determined by the angle β_{k+1} in the relative polar coordinate system. Let N_c equally spaced candidate edge points $\boldsymbol{r}_i = (d_i, \beta_{k+1})'$, $i = 1, \ldots, N_c$ are selected on the segment, limited by the imposed constraints. The edge magnitude of each point $\boldsymbol{r}_i$ is calculated according to the next filtering algorithm, similarly to [1]

$$F_{edge}(d_i, \beta_{k+1}) = \frac{1}{3}(1 - I(d_i, \beta_{k+1}))^2 \times \qquad (6)$$
$$I(d_i + 2\delta r, \beta_{k+1}) + I(d_i + \delta r, \beta_{k+1}) + I(d_i, \beta_{k+1}) -$$
$$I(d_i - \delta r, \beta_{k+1}) - I(d_i - 2\delta r, \beta_{k+1}) - I(d_i - 3\delta r, \beta_{k+1}),$$

where δr is a radial increment (a design parameter) and $I(\boldsymbol{r}_i)$ is the local grey-level normalised image intensity. The edge point with a maximum magnitude $\boldsymbol{r}_m = max\left\{F_{edge}(\boldsymbol{r}_i), i = 1, \ldots, N_c\right\}$ takes part in computation of the likelihood ratio. We propose the follow-

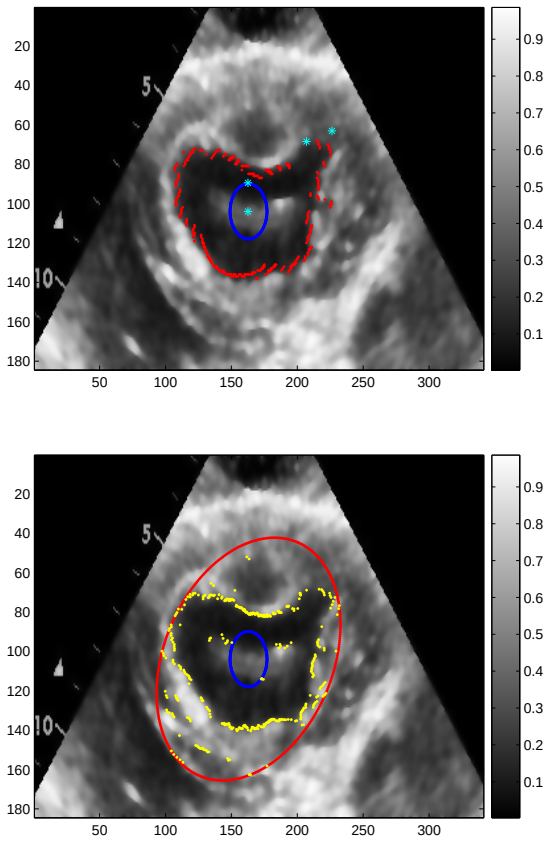

Fig. 4 (a) Detected edges with maximum magnitudes, (b) points with maximum gradient norms within the gating area

ing expressions for p_{on} and p_{off}

$$p_{on}(\widetilde{\boldsymbol{x}}_{k+1}^{(j)}) \propto \left|\nabla I(\widetilde{\boldsymbol{x}}_{k+1}^{(j)})\right|^2 exp\left\{-\frac{(\tilde{d}_{k+1}^{(j)} - d_m)^2}{2\sigma_e^2}\right\} \quad (7)$$

$$p_{off}(\widetilde{\boldsymbol{x}}_{k+1}^{(j)}) \propto exp - \frac{\left|\nabla I(\widetilde{\boldsymbol{x}}_{k+1}^{(j)})\right|}{\lambda}, \quad (8)$$

where $\widetilde{\boldsymbol{x}}_{k+1}^{(j)} = (\tilde{x}_{k+1}^{(j)}, \tilde{y}_{k+1}^{(j)}, \tilde{d}_{k+1}^{(j)}, \tilde{\beta}_{k+1}^{(j)})', j = 1, \ldots, N$, $\boldsymbol{r}_m = (d_m, \beta_{k+1})'$ and σ_e^2 is a design parameter. In the results, presented below, this parameter takes value of $\sigma_e^2 = 2$. The operation of the edge detector (6) is demonstrated in Fig. 4(a), where the detected edge points are coloured in red. The points with a maximum gradient norm along n equispaced radii within the gate are displayed in yellow (Fig. 4(b)). The likelihood ratio

$$\ell(\widetilde{\boldsymbol{x}}_{k+1}^{(j)}) = p_{on}(\widetilde{\boldsymbol{x}}_{k+1}^{(j)})/p_{off}(\widetilde{\boldsymbol{x}}_{k+1}^{(j)}), \quad (9)$$

is used for updating of the particle weights (3).

Likelihood II. In many cases, the grey-levels inside and outside the segmented object have well-marked distinct charachteristics. This valuable information can be incorporated into the segmentation process by an alternative way for the likelihood computation. Denote by $p_{in} \equiv p_{in}(\boldsymbol{y}(\boldsymbol{x}_k))$ the likelihood of the pixel $\boldsymbol{x}_k$, if it is inside the segmented area. Denote also by $p_{out} \equiv p_{out}(\boldsymbol{y}(\boldsymbol{x}_k))$ the likelihood of the same pixel, if it is outside the segmented region. The likelihood multiplier

$$\wp = p_{in} * p_{out}, \quad \wp \propto \frac{1}{p_{off}}, \quad \wp * p_{on} \propto p(\boldsymbol{y}(\boldsymbol{x}_k))$$

is a measure, extracting also useful information from the image data. Different grey-level distribution models have been used in the literature for ultrasound image segmentation, including Gaussian, Gamma, Beta, exponential, Rayleigh and mixture of Gaussian distributions [8,28,36]. Gamma distributions are a good choice due to their flexibility: a wide range of empirical distributions can be covered by fitting the data to the pdf with different shape and scale parameters (as shown on Fig. 3(b)).

Likelihood III.
In the cases of images with a non-homogeneous intensity distributions, it is difficult to obtain a suitable p_{off} or p_{out} distribution models. Then only p_{on} can be used as a measure, proportional to the likelihood function. We have explored the following modified likelihood p_{on}^m

$$p_{on}^m(\widetilde{\boldsymbol{x}}_{k+1}^{(j)}) \propto G(\widetilde{\boldsymbol{x}}_{k+1}^{(j)})^2 exp\left\{-\frac{(\tilde{d}_{k+1}^{(j)} - d_m)^2}{2\sigma_e^2}\right\},$$

where the gradient in x axis, respectively in y axis, for pixel $\boldsymbol{x}_k$ is calculated with the operator [39]

$$\begin{aligned} G_x(\boldsymbol{x}_k) =& I(x_k - 2, y_k) + 2I(x_k - 1, y_k) \\ & - 2I(x_k + 1, y_k) - I(x_k + 2, y_k) \quad (10) \\ G_y(\boldsymbol{x}_k) =& I(x_k, y_k - 2) + 2I(x_k, y_k - 1) \\ & - 2I(x_k, y_k + 1) - I(x_k, y_k + 2) \quad (11) \\ G(\boldsymbol{x}_k) =& \sqrt{G_x(\boldsymbol{x}_k)^2 + G_y(\boldsymbol{x}_k)^2}. \quad (12) \end{aligned}$$

One of these proposed likelihood functions can be used for computing the particle weights $\widetilde{w}_{k+1}^{(j)}, j = 1, \ldots, N$ (relationship (3)). The updated weights take part in the calculation of the current contour estimate

$$(\hat{\boldsymbol{x}}_{0:k+1}|\boldsymbol{y}) \approx \sum_{j=1}^{N} \widetilde{w}_{k+1}^{(j)} \widetilde{\boldsymbol{x}}_{0:k+1}^{(j)}.$$

4 Algorithm Outline

The proposed segmentation algorithm is implemented in three steps of preprocessing, filtering and smoothing.

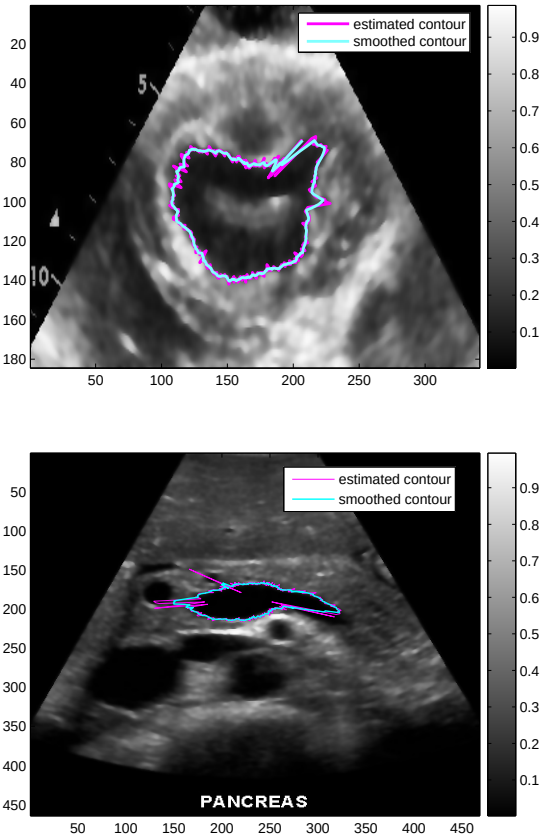

Fig. 5 Estimated and smoothed heart (a) and pancreas (b) contours, $N = 1000$

Preprocessing. A fundamental requirement of the noise filtering method is to preserve the important information for object boundaries [10]. A non-linear Gaussian filter, performing edge preserving diffusion has been adopted from [3, 5]. The processed ultrasound images have been smoothed by a filter chain with three stages and initial parameters $\sigma_x = 1.0$ and $\sigma_z = 0.25$.

Particle Filtering. A multiple model particle filter (MM PF) is realised having the particularity that each particle is a contour. With the recursive implementation $k = 0, 1, \ldots, n$ the number of points in each contour $\boldsymbol{x}_{0:k}^{(j)}, j = 1, \ldots, N$ increases consecutively, and hence increasing in this way the execution time. It is important to keep a minimum sample size N, achieving the minimum execution time. However, this leads to some roughness of the contour.

Smoothing. The MATLAB Curve Fitting Toolbox is used to smooth the contour curve. The estimated and smoothed (by standard moving average built-in procedure) heart and pancreas contours are presented in Fig.(5).

5 Segmentation Results

According to [28], "there is a general lack of standardization of performance measures". This makes difficult the quantitative validation of image segmentation algorithms. Since "there are also no standard databases on which deferent groups can compare methods", the quality of our segmentation algorithm is tested over a variety of simulated and real images, obtained by the Internet image database: for ultrasound tumor and lesion images ($http://smiswi.sasktelwebhosting.com$).

Design parameters. The selected sampling angle is $\triangle\beta = 1\ [deg]$, corresponding to $n = 360$ equally spaced radii. A MM PF with three models $s = 3$ is designed for estimating the contour state vector. Each model has different radial incitement, (Fig. 2): $\triangle d = 0$ for $m = 1$, $\triangle d = \gamma/4$, $(m = 2)$ and $\triangle d = -\gamma/4$ for $m = 3$, where $\gamma = Re_{max} - R_c$ is the aspect ratio. The standard deviation of the process noise $\mathrm{w}_k \sim \mathcal{N}(0, \sigma_d^2(m_k))$, modeling the perturbations in the distance increment is chosen equal to $\sigma_d = \gamma/16$, the same for all models. The filter is initialised with the exact coordinates of the starting point $\boldsymbol{x}_0$, as shown on Fig. 1. The initial mode probability vector of the Markov chain, governing the model switchings is as follows: $P_0 = (0.8, 0.1, 0.1)$. The transition probability matrix π has respectively the following diagonal $\pi_{ii} = 0.8$ and off-diagonal $\pi_{ij} = 0.1$ elements, $i, j = 1, 2, 3$. The threshold for resampling is $N_{thresh} = N/10$.

Segmentation results over simulated images. The ultrasound simulation package "Field II" [18] provides an excellent tool for testing newly developed ultrasound signal processing and segmentation algorithms. By means of "Field II", images with complex contours are generated in [19], Fig. 6(a). The image after being preprocessed with the non-linear Gaussian filter is given in Fig. 6(b). The operation of the proposed MM filter is demonstrated in Fig. 6(c). The filter is implemented with the *Likelihood II*, the radial increment is $\delta r = 5$ and the number of particles is $N = 800$. The results obtained with $N = 500$ and *Likelihood I* are similar.

The "Field II" package had been shown also efficiency in [20, 27] for simulating the output of the transducer, receiving signals from preliminary defined lesions (phantoms). Lesions with different shapes - circular, elliptical and Cassinian oval are designed to obtain echogenicity map of the phantoms. Next, the authors of [20, 27] developed and applied a combination of two noise reduction techniques, multi-angle spatial compound imaging (MACI) and coded excitation of the transducer, to improve the image quality. The image, generated by using

compounding and coded excitation with signal-to-noise ratio $SNR = 1$ $[dB]$ additive noise is shown in Fig. 7. The segmentation results, obtained by our MM PF with different sample sizes are given in the same Figure. The experiments show, that the number of particles depends mainly on the size of the gating area. The nearly circular form affords maintaining a smaller gate in comparison with the ellipse and Cassinian oval. Therefore, the same estimation quality is achieved with a smaller sample size.

An additional denoising wavelet based technique with soft thresholding as described in [21] leads to an additional improvement of the image quality, as shown on Figs. 8 (a) and (b). It can be seen from Fig. 8 (b) that the contours delineated by using *Likelihood II* are the best in this case of discernable intensities inside and outside the delineated areas.

Segmentation results over real images. The segmentation of a breast cyst, ovarianus, thyroid and pancreas are shown in Figs. 9 and 10. It can be seen from these figures, that the MM particle filtering algorithm produces convergent contours with a good estimation accuracy. Based on extensive experiments with the filter, we have made conclusions about the influence of the prior dynamics and measurement formation on the estimation process.

Number of initial starting points for contour segmentation. The number of initial starting points can be reduced to three or respectively to two, by using additional information from the image. In [4] a statistical procedure is proposed for automatic localisation of the starting point $\boldsymbol{x}_0$, based on the image gradient intensity. The number of the initial points can be further reduced to two if the foreground is significantly different than the background. For instance, breast lesion images have such well distinguishable and homogeneous regions. A piecewise estimate $\boldsymbol{x}_{min}$ is automatically determined in [4], based on the empirical intensity distribution inside and outside the lesion.

The suggested model of contour dynamics takes into account the convexity of the segmented regions. The experiments with more complex (higher order) dynamic models did not improve the estimation accuracy. However, the convexity assumption limits the application area: if the convexity is not fulfilled, deformations are possible, as it is obvious from Fig. (10 (c)), the right side of the upper contour.

Measurement model. The correct interpretation of the image data, namely the measurement formation process, has a great importance for the segmentation quality in this Bayesian context. Our experiments show, that the edge detection algorithm, proposed in [1, 2], is an excellent procedure, providing accurate results in almost all studied real and simulated images [19]. In [2], the smoothing capabilities of the PDA procedure (by calculating one weighted measurement from N_c edges with maximum magnitudes) provide a smooth contour estimate. The PDA incorporation into the MM PF framework is straightforward [6]. However, it is ac-

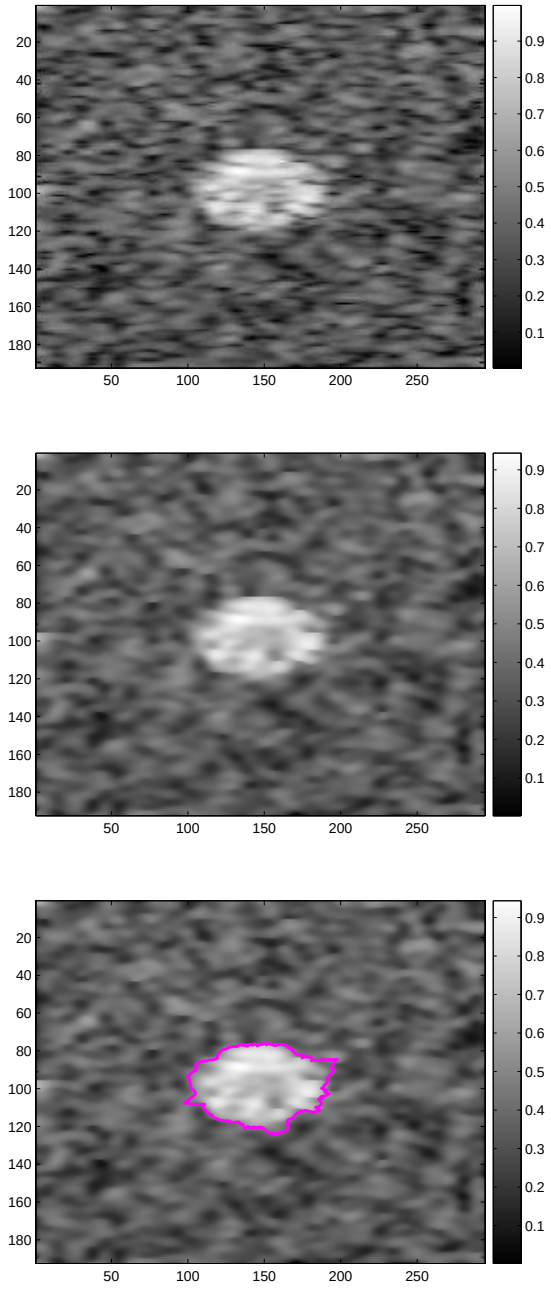

Fig. 6 Simulated image before (a) and after (b) preprocessing; (c) the estimated contour with $N = 800$ particles and $\delta r = 5$

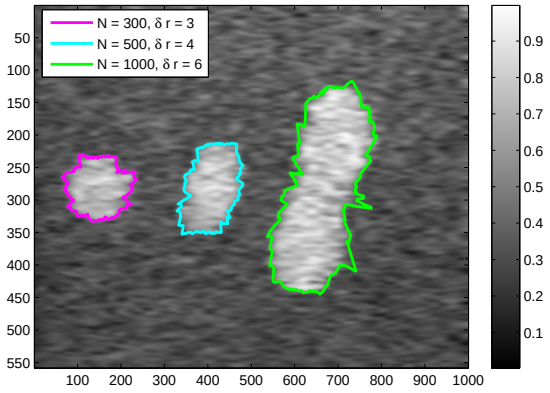

Fig. 7 Estimated contours of lesions with circular, elliptical and Cassinian oval forms

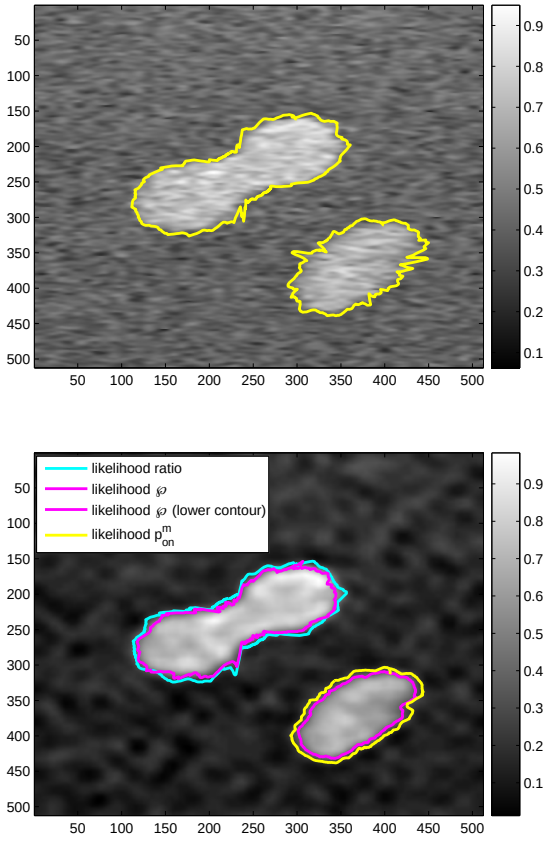

Fig. 8 (a) Segmentation results by using *Likelihood III*; (b) Comparison of the likelihoods.

companied with an increased computational time. In our implementation, the particle weight is proportional to its distance to the edge point with a maximum magnitude. The contour estimate is very sensitive to the abrupt contour changes, but at the cost of certain contour roughness, which is alleviated by the postprocessing step of smoothing.

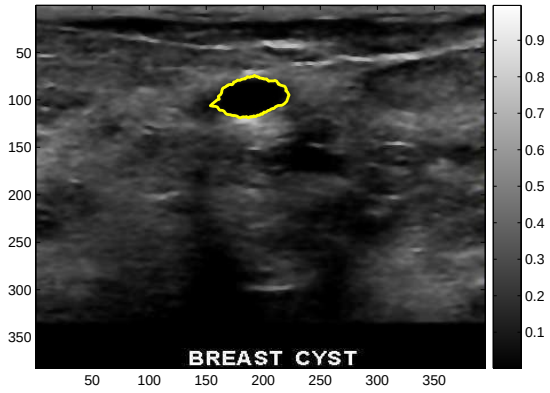

Fig. 9 Segmentation of a breast cyst

Sensitivity analysis. The proper choice of the seed point within the lesion area is a prerequisite to accurate segmentation results. We have explored the sensitivity of the segmentation algorithm to the seed point location. The displacements from the exact seed point location in the range of ±6 pixels do not affect the segmentation results. The multiple model structure of the tracking particle filter contributes to a great extend to this flexibility.

Execution time. The computational complexity is another important issue that we investigated. In the framework of the MATLAB environment, the processing time of a contour with $n = 365$ contour points and sample size $N = 500$ is approximately $t_{ex} = 5$ $[min]$ on a conventional PC (AMD Athlon(tm) 64 Processor 1.81 GHz). The execution time for $N = 800$ and $N = 1000$ is approximately $t_{ex} = 8$ $[min]$ and $t_{ex} = 10$ $[min]$. The contour quality is almost the same for $N = 500$, 800 and $N = 1000$. If the other design parameters are properly selected, the sample of $N = 500$ particles provides sufficient estimation accuracy. By using C++ programming tools the computational time can be additionally reduced.

6 Conclusions

A multiple-model particle filtering algorithm for segmenting contours in ultrasound medical images is proposed in this paper. Some of the advantages of the simulation-based Monte Carlo techniques are shown: multiple hypotheses governed contour dynamics and measurement gating based on constraints. The main novelty of this paper is in the proposed likelihoods that

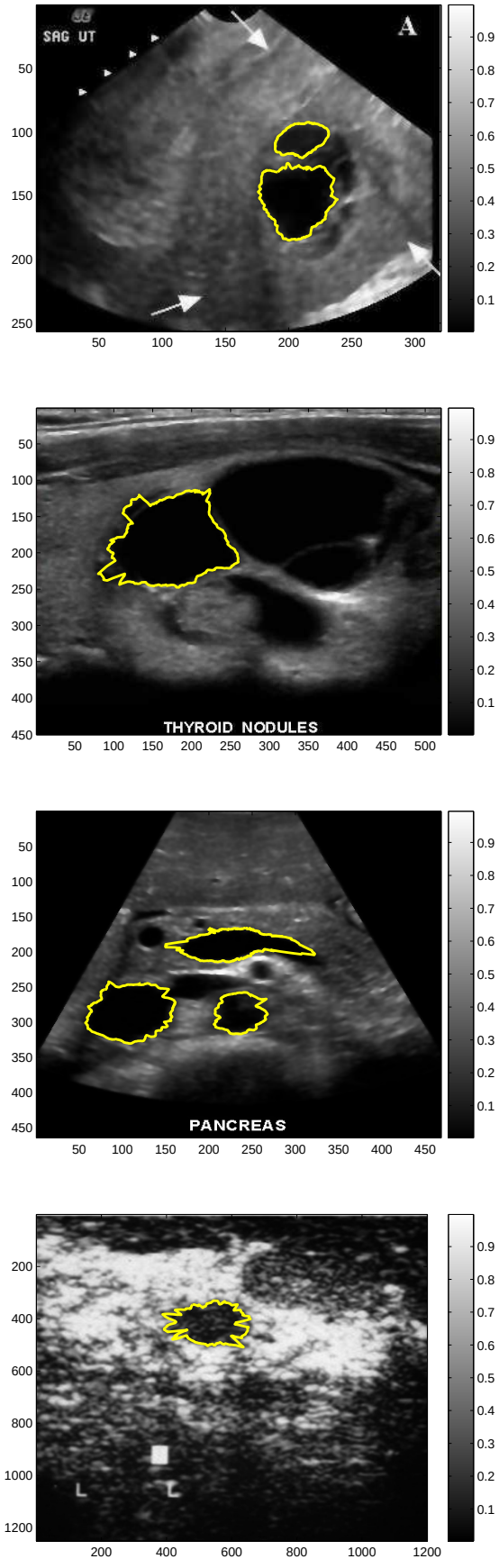

Fig. 10 Segmentation of (a) ovarianus, (b) thyroid (c) pancreas and (d) lesion images

integrate the features of the grey-level distributions inside and outside the segmented areas with intensity gradient information.

The algorithm can be applied to different types of images, including from medical applications. The restriction is related with the convexity of the segmented objects. In the general case, four manually selected points are necessary for its proper operation. However, if it is applied to a concrete clinical task, the number of necessary points could be reduced.

The algorithm performance is studied by segmenting contours from a number of real and simulated images, obtained by Field II [18], the ultrasound simulation program and additionally processed by several types of imaging techniques [20, 21, 27]. Very good estimation accuracy is achieved at the cost of acceptable computational complexity and convergence rate.

The Monte Carlo methods have a potential for classifying different types of lesions with high diagnostic confidence. Our further work will be focused on the important task of fully automated breast tumors segmentation with the possibility of distinguishing between benign and malignant tumors.

Acknowledgements The authors are thankful Prof. Behar [3] for recommending us the Gaussian filter, for her MATLAB implementation and valuable discussions. The authors are also grateful to the colleagues Dr. P. Konstantinova and Dr. M. Nikolov for providing us with the simulated images.

References

1. P. Abolmaesumi, M. Sirouspour, An Interacting Multiple Model Probabilistic Data Association Filter for Cavity Boundary Extraction from Ultrasound Images, IEEE Trans. on Medical Imaging, **23**(6), 772–784 (2004)
2. P. Abolmaesumi and M. Sirouspour, Segmentation of prostate contours from ultrasound images, Proc. of IEEE International Conference on Acoustics, Speech and Signal Processing, **3**, 517–520 (2004)
3. D. Adam, S. Beilin-Nissan, Z. Friedman, V. Behar, The combined effect of spatial compounding and nonlinear filtering on the speckle reduction in ultrasound images, Ultrasonics **44**, 166-181 (2006)
4. D. Angelova, L. Mihaylova, Contour Extraction from Ultrasound Images Viewed as a Tracking Problem, Proc. of the 12th International Conference on Information Fusion, Seattle, WA, USA, 284-291 (2009)
5. V. Aurich, J. Weule, Non-linear Gaussian filters performing edge preserving diffusion, 17th DAGM Symposium, Bielefeld, 538–545 (1995)
6. Y. Bar-Shalom, X. R. Li, Multitarget-Multisensor Tracking: Principles and Techniques, Storrs, CT:YBS Publishing (1995)
7. Y. Boers and J.N. Driessen, Point Estimation for Jump Markov Systems: Various MAP Estimators, Proc. 12th International Conf. on Information Fusion, 33-40 (2009)

8. E. Brusseau, E., C. L. de Korte, F. Mastik, J. Schaar, A. van der Steen, Fully automated endoluminal contour detection in intracoronary ultrasound images: a pre-processing for intravascular elastography, IEEE Proceedings, Ultrasonics Symposium, **2**, 1917–1920 (2002)
9. R. Cárdenes and R. de Luis-Garcia and M. Bach-Cuadra, Multidimensional Segmentation Evaluation for Medical Image Data, Computer Methods and Programs in Biomedicine, **96** (2), 108-124 (2009)
10. R. Chang, W. Wu, W. Moon, D. Chen, Automatic ultrasound segmentation and morphology based diagnosis of solid breast tumors, Journal Breast Cancer Research and Treatment, Springer, **89**:179–185 (2005)
11. V. Daanen, J. Tonetti, J. Troccaz, An Information Fusion Method for the Automatic Delineation of the Bone-Soft Tissues Interface in Ultrasound Images, LNCS **3117**, Springer, 218-229 (2004)
12. B. Dhalila, S. Y. Khoodoruth, H. C. S. Rughooputh, and W. Lefer, Semi-Automatic Integrated Segmentation Approaches and Contour Extraction Applied to Computed Tomography Scan Images, International Journal of Biomedical Imaging, **2008**: 1–11 (2008)
13. A. Doucet, N. de Freitas, N. Gordon, Sequential Monte Carlo Methods in Practice, Springer-Verlag, New York, USA, (2001)
14. A. Fan, J. Fisher, W. Wells, J. Levitt, A. Willsky, MCMC Curve Sampling for Image Segmentation, Maeder (Eds.): MICCAI 2007, Part II, LNCS **4792**, 477-485 (2007)
15. C. Florin, N. Paragios, J. Williams, Particle Filters, a Quasi-Monte Carlo Solution for Segmentation of Coronaries, LNCS, Springer, Vol. 3749, Medical Image Computing and Computer-Assisted Intervention MICCAI 2005, 246–253 (2005)
16. R. Goldenberg, R. Kimmel, E. Rivlin and M. Rudzsky, Fast Geodesic Active Contours, IEEE Trans. on Image Processing, **10**(10), 1467-1475 (2001)
17. G. Hamarneh, T. Gustavsson, Combining snakes and active shape models for segmenting the humanleft ventricle in echocardiographic images, IEEE Computers in Cardiology, **27**, 115–118 (2000)
18. J. Jensen, Field II Ultrasound Simulation Program, Technical University of Denmark, http://www.es.oersted.dtu.dk/staff/jaj/field/
19. P. Konstantinova, D. Adam, D. Angelova, V. Behar, Contour Determination in Ultrasound Medical Images Using Interacting Multiple Model Probabilistic Data Association Filter, LNCS 4310, Springer-Verlag, 628-636 (2007)
20. P. Konstantinova, V. Behar, M. Nikolov, A Comparison of Contour Determination in Ultrasound Medical Images Generated by two types of Imaging Techniques, Balkan Conference in Informatics, Bulgaria, 29–40 (2007).
21. P. Konstantinova, M. Nikolov, V. Behar, Ultrasound Image Enhancement via Wavelet Thresholding, Proceedings of the International Conference Automatics and Informatics, Sofia, Bulgaria, IV-5–IV-8 (2008)
22. X. Liu, and Nixon, M. (2007) Medical Image Segmentation by Water Flow. Proc. of Medical Image Understanding and Analysis MIUA 2007, UK (2007)
23. J. L. Marroquin, E. A. Santana, S. Botello, Hidden Markov Measure Field Models for Image Segmentation, IEEE Trans. Pattern Analysis and Machine Intelligence, **25**(11), 1380–1387 (2003)
24. M. Martin-Fernandez, C. Alberola-Lopez, An approach for contour detection of human kidneys from ultrasound images using Markov random fields and active contours, Medical Image Analysis **9**(1), 1-23 (2005)
25. M. Mignotte, J. Meunier, An unsupervised multiscale approach for the dynamic contour-based boundary detection issue in ultrasound imagery, Int. Conf. Computer Vision, Pattern Recognition and Image Processing, USA, **2**, 366–369 (2000)
26. M. Mignotte, J. Meunier, A multiscale optimization approach for the dynamic contour-based boundary detection issue, Computerized Medical Imaging and Graphics,**25**(3), 265–275 (2001)
27. M. Nikolov, V. Behar, Statistical Analysis of Image Quality in Ultrasound Imaging Systems with Coded Excitation, Intern. Workshop - Advances and Applications of Dezert-Smarandache Theory for Plausible and Paradoxical Reasoning for Information Fusion, Bulgaria, 32–38 (2006)
28. J. A. Noble, D. Boukerroui, Ultrasound Image Segmentation: A Survey, IEEE Trans. on Medical Imaging, **25** (8), 987–1010 (2006)
29. N. Otsu, A threshold selection method from gray level histograms, IEEE Trans. Systems, Man and Cybernetics, **9** (1), 62–66 (1979)
30. P. Pérez, A. Blake, and M. Gangnet, Jetstream: Probabilistic contour extraction with particles, Proc. Int. Conf. on Computer Vision (ICCV), **II**(5):524-531 (2001)
31. F.Pitié, A.Kokaram, R. Dahyot, Oriented Particle Spray: Probabilistic Contour Tracking with Directional Information, In Irish Machine Vision and Image Processing (IMVIP'04), Dublin, Ireland (2004)
32. W. Qua, X. Huangb, Y. Jiac, Segmentation in Noisy Medical Images Using PCA Model Based Particle Filtering, Proc. of the SPIE, **6914**, 69143I (2008)
33. B. Ristic, S. Arulampalam, N. Gordon, Beyond the Kalman Filter: Particle Filters for Tracking Applications, Artech House (2004)
34. F. Sahba, H. Tizhoosh, M. Salama, A coarse-to-fine approach to prostate boundary segmentation in ultrasound images, BioMedical Engineering, 4:58 (2005)
35. S. Saha, Y. Boers, H. Driessen, P.K. Mandal and A. Bagchi, Particle Based MAP State Estimation: A Comparison, Proc. 12th International Conf. on Information Fusion, 278–283 (2009)
36. G. Storvik, A Bayesian approach to dynamic contours through stochastic samplingand simulated annealing, IEEE Trans. Pattern Analysis and Machine Intelligence, **16**(10), 976–986 (1994)
37. P. Torr, A. Blake, et al., Bayesian Methods in Graphics, Proc. in the GraphCon 2003, Moscow State University (2003)
38. A. Tsai, W. Wells, S. Warfield, A. Willsky, An EM algorithm for shape classification based on level sets, Medical Image Analysis **9**, Elseiver, 491-502 (2005)
39. X. Xu and B. Li, Adaptive Rao-Blackwellized Particle Filter and Its Evaluation for Tracking in Surveillance, IEEE Trans. on Image Processing, **16**(3), 838–849 (2007)
40. W. Yao, P. Abolmaesumi, M. Greenspan, R. Ellis, An Estimation/Correction Algorithm for Detecting Bone Edges in CT Images. IEEE Trans. Med. Imaging **24** (8), 997–1010 (2005)
41. H. Zaidi, Medical image segmentation: Quo Vadis, Computer Methods and Programs in Biomedicine, Elsevier, **84**, 63-65 (2006)